Eur. Phys. J. D **28**, 435–445 (2004)
DOI: 10.1140/epjd/e2003-00316-1

THE EUROPEAN PHYSICAL JOURNAL D

First-order Fréedericksz transition and front propagation in a liquid crystal light valve with feedback

M.G. Clerc[1], T. Nagaya[2], A. Petrossian[3], S. Residori[4,a], and C.S. Riera[5]

[1] Departamento de Física, Facultad de Ciencias Físicas y Matemáticas, Universidad de Chile, Casilla 487-3, Santiago, Chile
[2] Department of Electrical and Electronic Engineering, Faculty of Engineering, Okayama University, Japan
[3] Physics Department, Yerevan St. University 1, A. Manoogian st. 375049 Yerevan, Armenia
[4] Institut Non Linéaire de Nice, UMR 6618 CNRS-UNSA, 1361 route des Lucioles, 065600 Valbonne, France
[5] DAMTP-CMS, Wilberforce Road, Cambridge CB3 0WA, UK

Received 1st August 2003 / Received in final form 21 October 2003
Published online 6 January 2004

Abstract. Fréedericksz transition can become subcritical in the presence of a feedback mechanism that leads to the dependence of the local electric field onto the liquid crystal re-orientation angle. We have characterized experimentally the first-order Fréedericksz transition in a Liquid Crystal Light Valve with optical feedback. The bistability region is determined, together with the Fréedericksz transition point and the Maxwell point. We show the propagation of fronts connecting the different metastable states and we estimate the front velocity. Theoretically, we derive an amplitude equation, valid close to the Fréedericksz transition point, which accounts for the subcritical character of the bifurcation.

PACS. 05.45.-a Nonlinear dynamics and nonlinear dynamical systems – 64.60.-i General studies of phase transitions

1 Introduction

Liquid crystals under the influence of electric and magnetic fields exhibit a large variety of complex dynamical behaviors, like electro-convection [1] and optical instabilities [2]. Pattern formation, defect dynamics and spatio-temporal instabilities have also been reported for a liquid crystal layer subjected to optical feedback, either in Liquid Crystal Light Valve (LCLV) experiments [3,4] or for a tilted liquid crystal cell with a feedback mirror [5–7].

One of the most well-studied phenomena in the physics of liquid crystals is the field-induced distortion of a homeotropic or planar aligned liquid-crystal film, called the Fréedericksz transition [8]. This transition is usually a second order one [9,10]. The possibility of modifying the Fréedericksz transition into a first-order one has attracted much attention not only in view of potential applications but also from the fundamental point of view of studying metastability and propagation of interfaces [11]. In order to render Fréedericksz transition first-order (subcritical bifurcation) several experiments have been considered during the last ten years, either through the simultaneous application of electric and magnetic field [12,13] or through the action of an optical field [14]. For a detailed review on optical Fréedericksz transition see reference [2] and the articles cited therein. Many of these experiments have shown an hysteresis cycle, either for liquid crystals possessing a very large optical anisotropy or for large intensities of the applied fields. Another approach, introduced in [15], is to realize a global feedback by means of a spatially integrated light intensity. Also in this case the Fréedericksz transition displays hysteresis, however spatial dynamics are lost as a consequence of the spatial averaging.

By using a LCLV with optical feedback, the first-order Fréedericksz transition may be studied by retaining the features of a spatially extended dynamics [16]. The nematic film is planar aligned and the feedback is provided by the LCLV photoconductor. Because of this feedback mechanism, the effective electric field applied locally across the liquid crystal layer depends on the liquid crystal director orientation, which, on its turn, depends on the electric field. As shown in [16], the first-order Fréedericksz transition is characterized by the presence of a large hysteresis region on the bifurcation diagram. Here we will focus our study on the propagation of interfaces (fronts) that connect the unstable and metastable states corresponding to the two branches of the bifurcation diagram.

The concept of front propagation, emerged in the field of population dynamics [17,18], has gained growing interest in biology [19], chemistry [20,21], physics [22–24] and

[a] e-mail: residori@inln.cnrs.fr

mathematics [25,26]. Front propagation for a first-order optical Fréedericksz transition has been theoretically studied in [11], where a model including hydrodynamic coupling with the director reorientation and transverse effects has been derived.

Domain segregation and coarsening have been reported for a LCLV with optical feedback in the case of a lateral shift in the feedback loop [27]. Chaotic domains have been observed for the same system in the case of a rotated and time-modulated feedback [28]. However, an experimental characterization of the front propagation in the vicinity of the first-order Fréedericksz transition has not yet been performed. In general, the study of fronts is not easily accessible from the the experimental side, whereas the LCLV with optical feedback is a good system for this kind of investigations.

The paper is organized as follows. In Section 2 we give an introduction to the Fréedericksz transition and we discuss its first-order features, with particular attention to the spatial dynamics. In Section 3 we present the experimental set-up and the light-driven feedback. Section 4 contains the derivation of the amplitude equation and the description of the measurement procedure used to determine the bifurcation diagrams. Section 5 is devoted to front propagation and reports the measurements of the front velocity. Section 6 are the conclusions.

2 The Fréedericksz transition

Fréedericksz transition is the elastic distortion of a nematic liquid crystal film under the action of a magnetic or electric field [8]. We will consider here the action of an electric field, but similar considerations and results can be obtained by substituting the electric field with a magnetic field and the dielectric tensor with the magnetic susceptibility. Fréedericksz transition is usually a second order transition (supercritical bifurcation) [9,10]. The possibility of modifying the Fréedericksz transition into a first-order one has been theoretically considered in [11], where transverse effects have been taken into account and front propagation has been predicted. Experimental evidence of the subcritical Fréedericksz transition on a spatially extended system has been given in [16] for a LCLV with optical feedback.

Liquid crystal materials are composed of anisotropic-shaped organic molecules. This results in the anisotropy of all their physical properties, especially optical properties [2]. In the nematic phase, the configuration of lowest energy is reached when all rod-like molecules are, on average, aligned along a single direction pointed out by a director $\vec{n}$ [9,10] and any description must include the symmetry $\vec{n} \leftrightarrow -\vec{n}$. This direction can be experimentally specified either by applying an external field, like an electric or magnetic one, or by imposing some particular boundary conditions at the confining surfaces of the sample, that is, the *anchoring* conditions. When two of these constraints are competing, the long-range orientational order may be partially destroyed.

For a sufficiently high magnitude of the applied field, the initial alignment due to the anchoring disappears in the bulk, that is, the system exhibits the Fréedericksz transition [8–10]. The threshold of this transition depends on the geometry of the set up, that is, on the orientation of the anchoring direction with respect to the external field. Besides, the chosen geometry determines the kind of uniform elastic distortion that appears in the medium at the onset of the transition.

2.1 The spatial dynamics in the subcritical case

The main feature of a first order transition is the appearance of hysteresis in the bifurcation diagram [29], that is, the system exhibits bistability for a certain parameter range. If the system is on one of these stable states and one begins to decrease the bifurcation parameter, then the state generically disappears (saddle-node bifurcation) or becomes unstable (pitchfork bifurcation) giving rise to the nucleation of other stationary stable states, which are largely different from the initial one. On the contrary, in second order transition the stable state that becomes unstable leads to the appearance of stationary stable states similar to the unstable one, i.e., the transition is a continuous one.

In a spatially extended system, a subcritical transition gives rise to a transient behavior characterized by front dynamics. For example, at the onset of bistability a large enough spatially localized perturbation can give rise to the appearance of the other stable state. As a consequence, the system displays a moving interface, so-called *front*, that connects the two stable states. A generic bifurcation diagram with reflection symmetry, together with the associated directions of the front propagation, is shown in Figure 1.

The front moves into the most energetically favorable state with a well defined velocity. In the case of one or two dimensional variational system and small interface curvature, the front velocity is proportional to the energy difference between the two states. This velocity can be modified by the curvature of the front, the so-called Gibbs-Thomson effect [30]. By increasing the bifurcation parameter, the metastable state becomes energetically equivalent to the other state, thus the front stops propagating. In this case, the system is said to be at the Maxwell point [31]. By further increase of the bifurcation parameter, the front velocity is reversed, that is, the most energetically favoured state invades the less favoured one.

Another interesting dynamical behavior appears when the state becomes unstable through a pitchfork bifurcation. Fluctuations of the initial state gives rise to the appearance of the other state. In this case there is a front connecting a stable state with an unstable one. This type of front is called Fisher-Kolmogorov-Petrosvky-Piskunov (FKPP) [17,18]. At variance with the normal front, the velocity of the FKPP front is not determined by the difference of energy between the two connected states. There is instead an infinite set of possible velocities, each one determined by the initial conditions [24,25]. At stationary

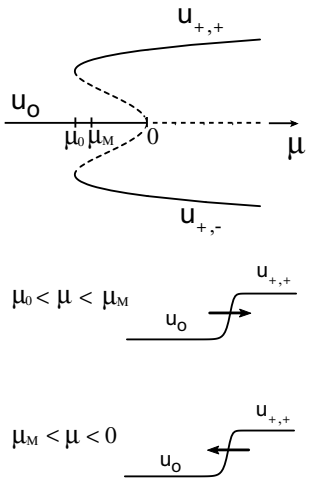

Fig. 1. The generic features of a subcritical bifurcation diagram and the associated directions of the front propagation. μ_0 and μ_M mark the beginning of the hysteresis region and the Maxwell point, respectively. The front connecting the u_0 to the $u_{+,+}$ state propagates towards the less stable state, this one being u_0 or $u_{+,+}$ depending on the value of the bifurcation parameter μ with respect to μ_M. The front dynamics are the same on the lower branch $u_{+,-}$.

state, the front velocity eventually reaches its minimum value, corresponding to the energy difference between the two states.

3 The experiment

3.1 The liquid crystal light valve

A LCLV was firstly used for feedback experiments by Akhmanov et al. [32]. The LCLV consists essentially in a nematic liquid-crystal film sandwiched between a glass plate and a photoconductive plate over which a dielectric mirror is deposed. A schematic diagram of the LCLV is shown in Figure 2. Coating of the two bounding plates induces a planar anchoring of the liquid crystal film, i.e., the nematic director $\vec{n}$ is parallel to the confining walls. Transparent electrodes covering the two plates, allow to apply an electric field across the liquid-crystal layer. The photoconductor behaves like a variable resistance, decreasing for increasing illumination. The equivalent electrical circuit is displayed in the bottom of Figure 2.

When the voltage V_0 is applied to the LCLV, liquid crystal reorientation takes place. The average angle θ of the director reorientation can be measured by sending a reading light beam on the front side of the LCLV and by measuring the phase shift $\Delta\varphi$ acquired by the light beam for travelling back and forth through the liquid crystal film. For doing this, a reference plane wave is used to make interference with the beam reflected by the LCLV. The phase shift is measured by recording onto a photodiode the displacement of the interference fringes.

The results are shown in Figure 3a as a function of the applied voltage V_0. Then, by fixing a value of the applied voltage $V_0 = 8\ V_{rms}$, the same measurements are repeated in the presence of a writing beam on the back side of the LCLV. The resulting additional phase shift $\Delta\varphi_{add}$ is plotted in Figure 3b as a function of the writing light intensity I_w. From the response curves, it appears that a large (greater than 2π) phase shift can be obtained in the LCLV either by changes of the applied voltage V_0 or by changes of the write beam intensity I_w. This means a large nonlinearity that can be controlled either electrically or optically. If the reading beam is sent back onto the write side of the LCLV, large feedback effects can be obtained. Indeed, the effective voltage applied across the

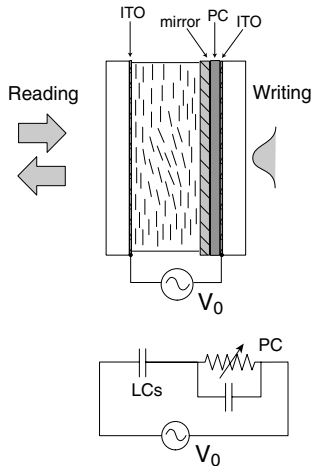

Fig. 2. The LCLV and its equivalent electrical circuit. The photoconductor PC behaves like a variable resistance controlled by the light intensity.

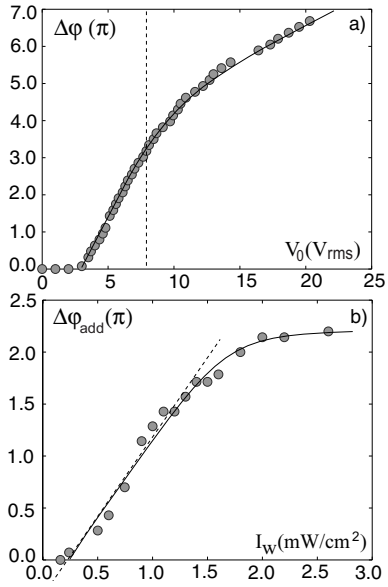

Fig. 3. Response of the LCLV: the phase shift $\Delta\varphi$ experienced by the reading light is measured (a) as a function of the applied voltage V_0 and (b) as a function of the writing light intensity I_w. Solid lines are guide for the eyes. In (b) $\Delta\varphi$ is the additional phase shift with respect to the one fixed by $V_0 = 8\ V_{rms}$. The dashed line is a linear fit, used to evaluate the response of the photoconductor.

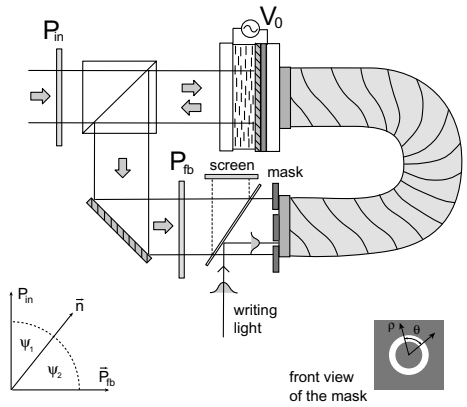

Fig. 4. Experimental set-up. Two confocal lenses, not displayed in the scheme, provide a 1:1 image-forming system from the front side of the LCLV to its rear side. The optical feedback loop is closed by a fiber bundle, which is aligned in order to avoid any rotation or shift. P_{in} and P_{fb} are, respectively, the input and feedback polarizer. Their orientation with respect to the liquid crystal director $\vec{n}$ is indicated in the left bottom of the figure. In the right bottom it is shown the mask used for the 1D experiments.

liquid crystal layer depends on the light intensity onto the photoconductor, and this one, on its turn, depends on the liquid crystal orientation, controlled by the voltage applied.

3.2 The light driven feedback

The experimental set-up for the light driven feedback is displayed in Figure 4. The optical loop is designed in such a way that the light beam experiences no diffraction as well as no geometrical transformation (the fiber bundle is adjusted in such a way that there is no rotation or translation of the feedback image). The light intensity I_w reaching the photoconductor is thus given by [3]

$$I_w = |\sin\psi_1 \sin\psi_2 + \cos\psi_1 \cos\psi_2 e^{-i\beta\cos^2\theta}|^2 I_{in} \qquad (1)$$

where $\beta\cos^2\theta$ is the overall phase shift $\Delta\varphi$ experienced by the light travelling forth and back through the liquid crystal layer. $\beta \equiv 2kd\Delta n$, $k = 2\pi/\lambda$ is the optical wave number, d is the thickness of the liquid crystal layer and Δn is the difference between the extraordinary ($\parallel$ to $\vec{n}$) and ordinary ($\perp$ to $\vec{n}$) index of refraction of the liquid crystal [9]. In our experiment, $\beta \simeq 60$ since $\lambda = 633$ nm, $\Delta n = 0.2$, $d = 15$ μm. $I_{in} = 1$ mW/cm^2 is the input light intensity, ψ_1 and ψ_2 are the angles formed by the input and feedback light polarization with the liquid crystal director $\vec{n}$, respectively. In most of the experiments we fix $\psi_1 = \psi_2 = 45°$, in order to maximize the birefringence of the LCLV.

The voltage V_0 applied to the LCLV is sinusoidal of frequency $f = 20$ kHz, much larger than the liquid crystal response time and the typical times for liquid crystal hydrodynamic instabilities [1]. This way, liquid crystals are sensitive only to the r.m.s value of the applied voltage and thereby perform only a static molecular re-orientation. However, backflow effects are to be taken into account when we deal with the spatial dynamics, since the motion of the interface between different orientations leads to a coupling with an hydrodynamic flow developing close to the front [11].

The effective electric field E_{eff} applied to the liquid crystal layer depends on the response of the photoconductor to the writing light intensity I_w and to the voltage V_0 applied to the liquid crystal layer. In the absence of light on the photoconductor, $E_{eff\,(I_w=0)} \equiv E_{(I_w=0)} = \Gamma E_0 = \Gamma V_0/d$, where V_0 is the total voltage applied to the LCLV, d is the liquid crystal thickness and $\Gamma < 1$ is a transfer factor that depends on the electrical characteristics (impedances) of the photoconductor, dielectric mirror and liquid crystal layers.

As long as the light intensity is sufficiently small, that is, of the order of a few mW/cm^2, the response of the photoconductor can be approximated by a linear function. Under this approximation, the total effective electric field applied to the liquid crystal film can be expressed as $E_{eff} = E_{(I_w=0)} + \alpha I_w$, where α is a phenomenological dimensional parameter that we can evaluate from the experimental characteristics of the LCLV (see Fig. 3). Indeed, by fitting the additional phase shift $\Delta\varphi_{add}$ as a function of the write intensity and by measuring I_w in mW/cm^2, we get $\Delta\varphi_{add} \simeq \tilde{\alpha} I_w$ with $\tilde{\alpha} = 4.0$ cm^2/mW. By fitting the fixed phase shift imposed by the applied voltage V_0, we get $\Delta\varphi \simeq \tilde{g} V_0$ with $\tilde{g} = 1.9$ V^{-1}. The total phase shift, $\Delta\varphi_{tot}$, is thus given by $\Delta\varphi_{tot} = \Delta\varphi + \Delta\varphi_{add} \simeq \tilde{g}[V_0 + (\tilde{\alpha}/\tilde{g}) I_w]$ where $\tilde{\alpha}/\tilde{g} = 2.1$ V cm^2/mW. Normalizing to the thickness d of the liquid crystal film, we have that a light intensity I_w on the photoconductor is equivalent to an additional applied electric field αI_w, with $\alpha = \tilde{\alpha}/\tilde{g}d = 0.70$ kV cm/mW.

4 The subcritical bifurcation

4.1 Derivation of the amplitude equation

The competition between the elastic restoring force and the electric torque for a nematic film is described by the Frank free energy [9]. In the LCLV, as a consequence of the optical feedback, the local electric field $\vec{E}$ depends on the director $\vec{n}$. Thus, the variation $\delta\mathcal{F}$ of the free energy, resulting from of a variation $\delta\vec{n}$ of the director, takes the form

$$\delta\mathcal{F} = \frac{1}{2}\int \delta\left[K_1\left(\vec{\nabla}\cdot\vec{n}\right)^2 + K_2\left(\vec{n}\cdot\left(\vec{\nabla}\wedge\vec{n}\right)\right)^2\right] d^3x$$
$$+ \frac{1}{2}\int \delta\left[K_3\left(\vec{n}\wedge\left(\vec{\nabla}\wedge\vec{n}\right)\right)^2\right] d^3x - \int \vec{E}\delta\vec{D}\,(\vec{n})\, d^3x, \qquad (2)$$

where K_1, K_2 and K_3 are the elastic constants describing the elastic deformation of the nematic film for splay, twist and bend, respectively, and the last integral accounts for

the electromagnetic contribution. The displacement vector $\vec{D}$ is related to the director by $\vec{D} = (\epsilon_\perp/2)\vec{E}(\vec{n}) + (\epsilon_a/2)(\vec{n}\cdot\vec{E}(\vec{n}))\vec{n}$, with ϵ_a being the dielectric anisotropy and $\epsilon_\perp$ the perpendicular dielectric permeability.

The variation of the displacement vector is

$$\delta\vec{D} = \frac{\epsilon_\perp}{2}\frac{\partial\vec{E}(\vec{n})}{\partial\vec{n}}\delta\vec{n} + \frac{\epsilon_a}{2}\left(\delta\vec{n}\cdot\vec{E}(\vec{n})\right)\vec{n} + \frac{\epsilon_a}{2}\left(\vec{n}\cdot\vec{E}(\vec{n})\right)\delta\vec{n} + \frac{\epsilon_a}{2}\left(\vec{n}\cdot\frac{\partial\vec{E}(\vec{n})}{\partial\vec{n}}\delta\vec{n}\right)\vec{n}$$

where $\partial\vec{E}/\partial\vec{n}$ is a tensor of order two with $(\partial\vec{E}/\partial\vec{n})_{i,j} = \partial E_i/\partial n_j$. The dynamical equation for the liquid crystal director is given by

$$\gamma\vec{n}\wedge\partial_t\vec{n} = -\vec{n}\wedge\frac{\delta\mathcal{F}}{\delta\vec{n}}, \quad \vec{n}\cdot\vec{n} = 1$$

where γ is the rotational viscosity of the nematic film.

For the sake of simplicity, we assume $K_1 = K_2 = K_3 = K$. Thus, the dynamical equation reads

$$\gamma\partial_t\vec{n} = K\left[\nabla^2\vec{n} - \vec{n}\left(\vec{n}\cdot\nabla^2\vec{n}\right)\right] + \epsilon_a\left(\vec{n}\cdot\vec{E}\right) \times\left[\vec{E} - \vec{n}\left(\vec{n}\cdot\vec{E}\right)\right] + \frac{\epsilon_\perp}{4}\frac{\partial\vec{E}^2}{\partial\vec{n}} - \frac{\epsilon_\perp}{4}\left[\vec{n}\cdot\frac{\partial\vec{E}^2}{\partial\vec{n}}\right]\vec{n} + \frac{\epsilon_a}{2}\left(\vec{n}\cdot\vec{E}\right)\left[\frac{\partial\vec{E}}{\partial\vec{n}}\cdot\vec{n} - \left(\vec{n}\cdot\left(\frac{\partial\vec{E}}{\partial\vec{n}}\cdot\vec{n}\right)\right)\vec{n}\right], \tag{3}$$

where $(\partial\vec{E}/\partial\vec{n})\cdot\vec{n} = n_x\vec{\nabla}E_x + n_y\vec{\nabla}E_y + n_z\vec{\nabla}E_z$.

At rest (without any electric field applied), the liquid crystal alignment is planar, that is, all the molecules are parallel to the x-axis (x and y being in the plane of the confining plate and z perpendicular to it), so that $\vec{n} = (1,0,0)$. In the presence of an electric field applied along z, $\vec{E} = (0,0,E_z)$ with $E_z = E(\vec{n}) = E_{(I_w=0)} + \alpha I_w(\vec{n})$, and for $\epsilon_a > 0$, the director reorients in the $(x{-}z)$-plane. As a consequence, the director becomes $\vec{n} = (n_x, 0, n_z)$ with $n_x^2 + n_z^2 = 1$.

After substituting the write intensity I_w, equation (1), in the expression for the electric field, we obtain

$$E(\vec{n}) = E_{(I_w=0)} + \alpha I_w(\vec{n}) = E_{(I_w=0)} + \alpha I_{in}\left[A + B\cos(\beta\cos^2\theta)\right] \tag{4}$$

where

$$A = \frac{1}{4}[\cos 2(\psi_1-\psi_2) + \cos 2(\psi_1+\psi_2) + 2],$$

$$B = \frac{1}{4}[\cos 2(\psi_1-\psi_2) - \cos 2(\psi_1+\psi_2)].$$

Close to the onset of the Fréedericksz transition, the director reorientation can be expressed as a Fourier series $n_z(x,y,z,t) = \sum_n u_n(x,y,t)\sin(n\pi z/d)$. For a small reorientation angle, the director reorientation along the z-direction, n_z, describes quite well the orientation angle of the liquid crystal molecules. By means of the standard bifurcation theory [24], it is possible to derive an amplitude equation for the first unstable Fourier mode, $n_z = u(x,y)\sin(\pi z/d)$ and $n_x = 1 - u^2\sin^2(\pi z/d)/2$. The amplitude equation reads

$$\partial_t u = c_1 u + c_3 u^3 + c_5 u^5 + \frac{K}{\gamma}\nabla_\perp^2 u \tag{5}$$

where the development has been extended up to the fifth order since the third order coefficient c_3 can become positive depending on the parameters of the system.

The amplitude equation, equation (5), describes qualitatively the subcritical bifurcation close to the transition point. The coefficients c_1, c_3 and c_5 are functions of the physical parameters of the experiments, that is, c_1, c_3 and c_5 are functions of β, $\epsilon_\perp$, ϵ_a, E_0, I_{in}, ψ_1, ψ_2. The three coefficients may change sign depending on the parameters set in the experiment, and in particular the sign of c_3 depends on the polarization angles ψ_1 and ψ_2 [16]. Note that A and B are periodic in ψ_1 and ψ_2, so that changing the polarizer angles modulates the response of the LCLV. When c_3 is negative and of order one, equation (5) describes a second order Fréedericksz transition. This transition becomes of a first order one when c_1 and c_3 are positive (and small) with c_5 negative. The complete expression of the coefficients is reported in the appendix.

4.2 Measurement of the bifurcation diagram

In order to observe the FT and to construct the experimental bifurcation diagram, the intensity I_w reaching the photoconductor is measured by extracting a small portion of the feedback light and by sending it onto a photodiode.

When the applied voltage V_0 is below the threshold for molecular reorientation, I_w has a value fixed by β. When reorientation occurs, we expect this value to change according to expression given in equation (1). We verify the validity of this prediction by measuring I_w in the absence of feedback, that is, by blocking the entrance of the fiber bundle with a black screen. The Fréedericksz transition takes place at $V_0 \simeq 3.2V_{rms}$.

When we remove the blocking screen, I_w changes according to the liquid crystal reorientation. Variations of I_w induce, on their turn, variations of the effective voltage applied across the liquid crystal film and hence a further reorientation. Once feedback is established between the applied voltage and the liquid crystal director, the FT becomes a first-order transition. A typical bifurcation diagram, recorded for $\psi_1 = \psi_2 = 45°$, is shown in Figure 5. The transition from the non oriented state to the oriented one is characterized by a large hysteresis region.

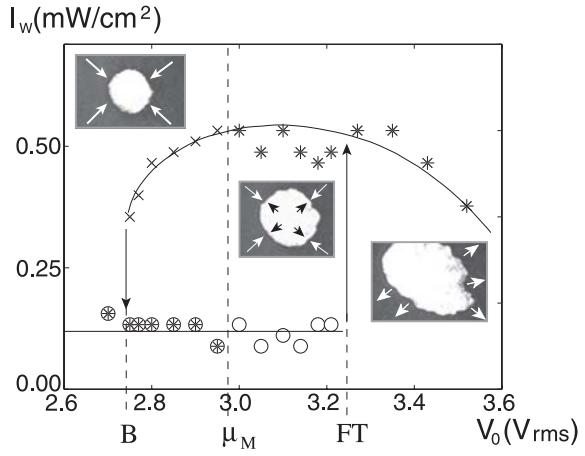

Fig. 5. I_w as a function of the applied voltage V_0: open circles are dark states with writing light off; stars are white states with writing light off; cross are white states with writing light on. The white state shrinks to zero or expands to infinity depending on the initial location of the perturbation. Beyond (and close to) the Maxwell point it exists a critical droplet radius for which the front velocity is zero.

4.3 Experimental results and qualitative comparison with the model

In Figure 5, I_w is plotted as a function of V_0 and in the presence of feedback. The transition point is characterized by an abrupt change in the intensity, which reaches its maximum value. Note that I_w is measured by a small area photodiode, i.e., it is a local measurement taken at the center of the feedback beam. By looking at the entire image of the beam with a CCD camera, we see that the transition point is characterized by a white spot developing over a dark background. Three representative images of the feedback field are displayed in Figure 5, showing the direction of the front propagation in dependence on the mutual stability of the white and the dark states. The dashed line marks the Maxwell point. Below this point the white state is less stable than the dark one and the white spot, once created by the writing light, contracts to zero.

Above the Fréedericksz transition point, the white spot nucleates spontaneously and the front expands until the white state covers all the background. In between, the front expands or retracts depending on the size of the perturbation. By increasing V_0 beyond the Fréedericksz transition point, the LCLV birefringence changes and the white state becomes *grey* until the dark value is reached again. Successive transitions to the white state are present for larger values of V_0.

By decreasing the voltage, we observe a hysteresis cycle. In order to determine the size of the bistable region, we inject an additional light spot (low power He–Ne laser) into the feedback loop. This acts as a small perturbation, triggering the transition from the dark state to the white one. The white state persists when we block the additional writing light, while it switches to the dark state if we perturb the feedback. In Figure 5, the arrows delimit the region over which this writing-erasing procedure is robust.

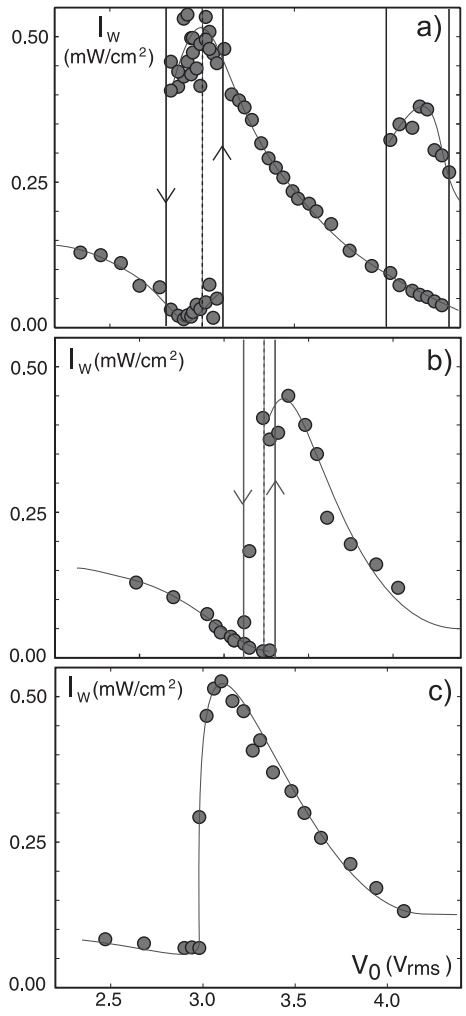

Fig. 6. Experimental bifurcation diagrams recorded for three different values of the polarizer angle: (a) $\psi_1 = \psi_2 = 45°$, (b) $\psi_1 = 45°$ and $\psi_2 = 38°$, (c) $\psi_1 = 45°$ and $\psi_2 = 18°$. Arrows mark the limits of the hysteresis region, dashed lines indicate the Maxwell point and thin lines are guides for the eyes. In (c) the bifurcation has become a second-order one.

The three crucial points, i.e., the beginning of the bistability, B, the Maxwell point, μ_M, and the Fréedericksz transition point, FT, are also identified by the divergence of the response times, as it was shown in [16].

In Figure 6 three experimental bifurcation diagrams are shown for different values of the polarizer angles ψ_2, while ψ_1 is fixed to 45°. The character of the bifurcation changes from a subcritical one (Fig. 6a) to a supercritical one (Fig. 6c), through a decreasing width of the hysteresis region (Fig. 6b). Note in Figure 6a the existence of a successive bifurcation after the Fréedericksz transition one, taking place at $V_0 = 3.90 V_{rms}$.

As it can be seen from the expression of the coefficients of the amplitude equation, equation (5), a change of ψ_1 and ψ_2 leads to a sign reversal of c_3 and c_5. We have substituted the experimental values of ψ_1 and ψ_2 in the expression for the coefficients and we have verified that the amplitude equation gives bifurcation diagrams which are

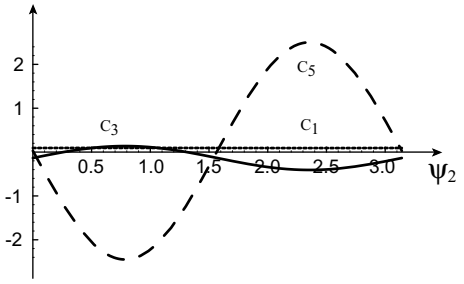

Fig. 7. Coefficients c_1 (dotted line), c_3 (continuous line) and c_5 (dashed line) as a function of the polarizer angle ψ_2 (radians). The system is close at the onset of the bifurcation, that is, c_1 is close to zero, and $\psi_1 = \pi/4$.

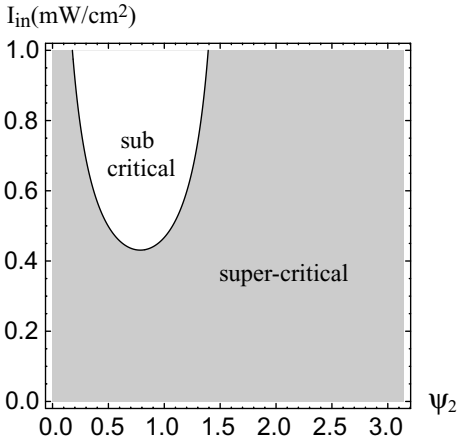

Fig. 8. Phase diagram as a function of the input intensity I_{in} and of the polarizer angle ψ_2 (radians). Solid line corresponds to $c_3 = 0$, marking the border between the subcritical and the supercritical case.

in a good qualitative agreement with the measured ones. In particular, it is possible to relate the character of the experimental bifurcations with the value of the coefficients, as we show in Figure 7, where c_3 and c_5 are reported as a function of ψ_2 and for a fixed value of $\psi_1 = 45°$. The first coefficient c_1 is set close to zero in order to keep the system close to the transition point.

The other parameters are fixed at the experimental values. As we can see on the plot, c_3 becomes positive for small values of ψ_2, whereas c_5 is already negative, thus assuring the saturation of the amplitude.

In Figure 8 it is shown a phase diagram in the plane of the input light intensity I_{in} and of the polarizer angle ψ_2. The applied electric field E_0 is computed in order to set the system at the bifurcation point, that is, at $c_1 = 0$. Then, we look at the sign of c_3 to determine whether the bifurcation is subcritical or supercritical. The line marks the transition between the two cases, corresponding to $c_3 = 0$. The phase diagram characterizes entirely the dependence of c_3 from the physical parameters that are readily accessible from the experimental side. Changing the value of c_3 leads to tuning the character of the Fréedericksz transition, from a largely subcritical one to a small subcriticality or even to supercriticality. In other words, an experimental procedure has been identified which allows to move the system along the tricritical point of the associated phase diagram. It is important to remark that in the general case of nascent bistability the bifurcation is associated to a cusp catastrophe in the space of parameters. However, this picture can change when the system presents a symmetry, like the reflection symmetry, as it occurs for the Fréedericksz transition (the reoriented state u is equivalent to the $-u$ state). In this case the catastrophe becomes smooth, like it is shown in Figure 8, at variance with the cusp singularity.

5 Front propagation

5.1 Features of the first-order model

In order to describe the dynamics associated to the amplitude equation, equation (5), we introduce the scaling

$$u = U_0 u', \quad t = T_0 t', \quad \text{and} \quad r = R_0 r'.$$

Omitting the primes, the amplitude equation reads

$$\partial_t u = \mu u + u^3 - u^5 + \nabla_\perp^2 u \tag{6}$$

where $U_0 = (c_3/c_5)^{1/2}$, $T_0 = c_5/c_3^2$, $R_0 = K\left(c_5/c_3^2\right)$ and $\mu = c_1 c_5/c_3^2$.

Therefore, the bifurcation is characterized by only one parameter, the bifurcation parameter μ. In Figure 1 it is shown the bifurcation diagram of the above equation. For negative μ and large enough amplitude ($\mu < -0.25$), the system has only one stable state $u(x,t) = u_0 = 0$. This state corresponds to a planar unperturbed alignment of the liquid crystal film. When the bifurcation parameter is increased, this solution become unstable for positive μ. The transition is a subcritical pitchfork bifurcation. In our case it corresponds to a first-order Fréedericksz transition. As a consequence of this transition, for $-1/4 \leq \mu \leq 0$ the previous model exhibits bistability and the stationary solutions are given by

$$\begin{aligned} u_0 &= 0, \\ u_{+,\pm} &= \pm\frac{\sqrt{1+\sqrt{1+4\mu}}}{2}, \\ u_{-,\pm} &= \pm\frac{\sqrt{1-\sqrt{1+4\mu}}}{2}. \end{aligned}$$

The states u_0 and $u_{+,\pm}$ are stable whereas and $u_{-,\pm}$ are unstable. We note that equation (6) is a variational one and is characterized by the potential

$$V(u) = -\mu\frac{u^2}{2} - \frac{u^4}{4} + \frac{u^6}{6}.$$

For $\mu = \mu_M = -3/16$, that is, at the Maxwell point, the system satisfies $V(u_0) = V(u_{+,\pm})$ [29].

Once these three critical points (beginning of the bistability B, Maxwell point μ_M and FT transition point)

are determined on the bifurcation diagram, the front dynamics is entirely characterized. For $-1/4 \leq \mu \leq 0$, the system has seven main fronts between $\{u_0; u_{+,\pm}\}$, $\{u_{+,\pm}; u_{+,\mp}\}$, $\{u_0; u_{-,\mp}\}$, and $\{u_{+,\pm}; u_{-,\pm}\}$, respectively. For $-1/4 < \mu < \mu_M$, the fronts $\{u_0; u_{+,\pm}\}$ propagate towards $u_{+,\pm}$, respectively. Correspondingly, if the planar state is perturbed enough, the system relaxes quickly to different domains between the stable states, and later on the less favorable domains disappear. For $\mu_M < \mu < 0$, the direction of front propagation is reversed. At the bifurcation point, $\mu = 0$, the fronts connect an unstable and a stable state, so that they belong to the class of FKPP fronts.

5.2 1D experiments: measurement of the front velocity

In order to minimize the influence of the 2D curvature onto the front velocity, we have performed quasi-1D experiments. A ring-shaped mask is introduced in the optical set-up, in contact to the entrance side of the fiber bundle.

The ring shape of the mask constraints the system to be quasi-1D and to satisfy periodic boundary conditions [33]. The choice of the ring is for the sake of simplicity, but any closed and smooth domain leads to similar results for the front velocity. The inner diameter D of the ring was chosen in between 5 and 10 mm whereas the ring thickness l was in between 0.5 and 1 mm, so that the aspect ratio D/l is quite large and the system can be considered as 1D. The large curvature of the ring mask is considered not to affect the front propagation that develops in the transverse direction. Moreover, the ring thickness is considered large enough not to introduce relevant boundary effects.

The velocity of the front propagating between the two differently oriented states has been measured by means of a computer controlled synthesizer. The control parameter V_0 is scanned along the hysteresis region and a standard movie of the front propagation along the ring is recorded at the same time. Instantaneous snapshots recorded for $V_0 = 3.05V_{rms}$ are shown in Figure 9.

Above the Maxwell point, V_0 is switched on from zero and the front nucleates over any inhomogeneities present in the LCLV. To see the front propagation below the Maxwell point, the initial condition for V_0 is chosen in the region of well developed reorientation and then V_0 is switched to a lower value, below Maxwell point. In this case, the front velocity is reversed and the white state contracts to zero. Instantaneous snapshots recorded for $V_0 = 2.84V_{rms}$ are shown in Figure 10.

Either below or above the Maxwell point, the front velocity is measured by unfolding the rings over a line and by constructing the corresponding spatio-temporal diagrams, as shown in Figure 11. The front velocity can be evaluated by measuring the ratio between the horizontal (space — x) and vertical (time — t) displacements. Note that LCLV inhomogeneities introduce a pinning of the front in particular spatial locations, so that the front stops or largely slow down at these places. When measuring the front velocity, we have considered only the slopes of the first linear portions on the spatio-temporal plots. Pinning of the front over LCLV inhomogeneities is also responsible for the stripe patterning which appears on the spatio-temporal plots.

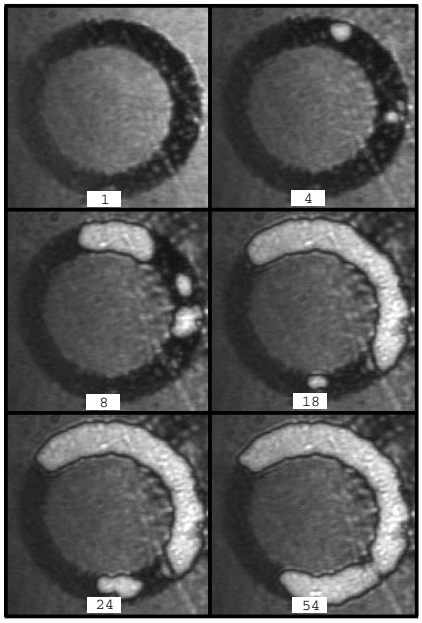

Fig. 9. Snapshots of the front propagation, recorded at $V_0 = 3.05V_{rms}$, above the Maxwell point. The successive instant times (in seconds) are indicated in the white labels.

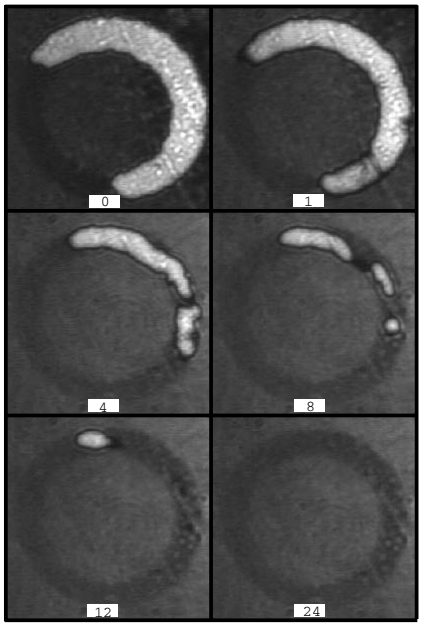

Fig. 10. Snapshots of the front propagation, recorded at $V_0 = 2.84V_{rms}$, below the Maxwell point. The successive instant times (in seconds) are indicated in the white labels.

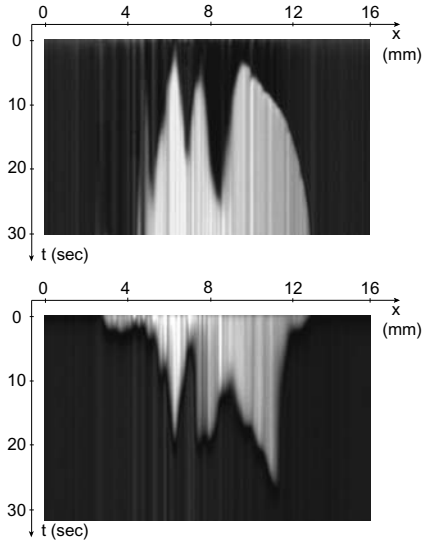

Fig. 11. Spatiotemporal plot showing the propagation of the front at (a) $V_0 = 3.05V_{rms}$, above the Maxwell point, and (b) $V_0 = 2.84V_{rms}$, below the Maxwell point.

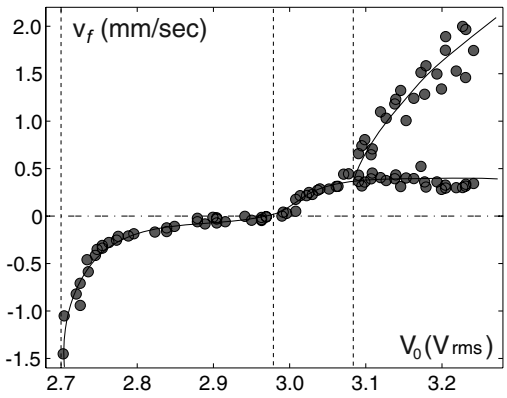

Fig. 12. Front velocity as a function of the bifurcation parameter V_0. Solid lines are guides for the eyes. Dashed lines mark the three critical points: B, μ_M, FT.

The resulting front velocities are plotted in Figure 12 as a function of the applied voltage V_0. On this figure, it is easy to identify the Maxwell point, where the front velocity goes to zero, and the FT point, beyond which the fronts become of a FKPP type. The regime of FKPP fronts is characterized by a transient propagation with a quite high velocity, which then relaxes to the minimal one. In Figure 12 the transient and the steady-state velocities correspond to the upper and lower branch, respectively. A spatio-temporal diagram for a FKPP front is shown in Figure 13, where it is possible to distinguish the nonlinear transient characterizing the early times of the front propagation.

6 Conclusions and discussions

We have studied the first-order Fréedericksz transition in a LCLV with optical feedback and we have developed a model which is in good qualitative agreement with the experimental observations. In particular, we have investigated the spatial dynamics related to front propagation and we have measured the velocity of the fronts in the case of quasi-1D experiments.

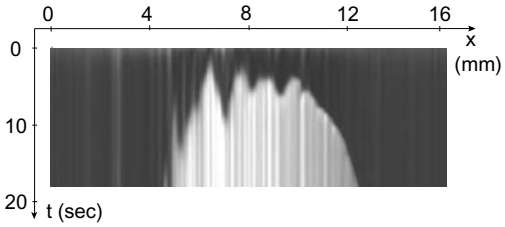

Fig. 13. Spatiotemporal plot showing the propagation of a FKPP front ($V_0 = 3.23V_{rms}$).

The theoretical model provides all the main qualitative features of the front dynamics. For $\mu_M \leq \mu \leq 0$, the model predicts fronts of the $\{u_0; u_{+,\pm}\}$ type which propagate towards the planar state u_0. For $\mu > 0$, the system presents FKPP fronts between the states $\{u_0; u_{+,\pm}\}$. These two kind of fronts have been studied in the experiment. However, a quantitative comparison with the measured values of front velocities would requires a more complete analysis, taking into account the backflow effects arising at the interfaces between differently oriented domains. We expect these effects to introduce an effective viscosity, that would renormalized the front velocity, as it was shown for an optical Fréedericksz transition [11]. Work is in progress in order to include backflow effects in our model.

Finally, note that spatial inhomogeneities and other noise sources can influence the stability of the two bifurcated states, so that the experimentally determined Maxwell point could indeed be slightly shifted from its real position. Another drawback of the experimental procedure is that it does not allow to distinguish between the two symmetric liquid crystal reorientations θ and $-\theta$. Indeed, the measured quantity, i.e. the intensity I_w, is related to θ through the function $\cos^2(\theta)$. A quantity sensitive to the sign of θ would instead lead to a bifurcation diagram with two symmetric branches, as the one shown in Figure 1. However, in the LCLV there is a small symmetry breaking related to the rubbing direction on the surfaces, so that a preferential selection of one of the two possible states is induced. Thus, the bifurcation is an imperfect one. From the experimental side, this is confirmed by the absence of dark walls, that would instead appear to separate domains of opposite reorientation.

The *Simulation Software* developed at INLN has been used for the study of the normal form equation, equation (5). M.G.C. thanks the support of Programa de inserción de científicos Chilenos of Fundación Andes, FONDAP grant 11980002 and FONDECYT project 1020782. A.P. acknowledges support from CNRS. This work has been supported by the ACI Jeunes of the French Ministry of Research (2218 CDR2).

Appendix

The complete expression of the coefficients in equation (5) is as follows. For sake of simplicity, we rename

$$E_{(I_w=0)} \equiv \tilde{E}_0$$

and we normalize all the coefficients by the rotational viscosity γ and the dielectric anisotropy ϵ_a

$$\begin{aligned}
\frac{\gamma}{\epsilon_a}c_1 = &-\frac{\pi^2}{d^2}\frac{K}{\epsilon_a} + \tilde{E}_0^2 \\
&+ 2A\alpha I_{in}\tilde{E}_0 + A^2(\alpha I_{in})^2 \\
&+ B\alpha I_{in}\left(\tilde{E}_0 + A\alpha I_{in}\right)\left(2\cos\beta + \frac{\epsilon_\perp}{\epsilon_a}\sin\beta\right) \\
&+ \frac{1}{2}B^2\left(\alpha I_{in}\right)^2\left[(1+\cos 2\beta) + \frac{\epsilon_\perp}{\epsilon_a}\beta\sin 2\beta\right]
\end{aligned}$$

$$\begin{aligned}
\frac{3\gamma}{\epsilon_a}c_3 = &\frac{\pi^2}{d^2}\frac{K}{\epsilon_a} - 2\tilde{E}_0^2 \\
&- 4A\alpha I_{in}\tilde{E}_0 - 2A^2(\alpha I_{in})^2 \\
&+ B\alpha I_{in}\left(\tilde{E}_0 + A\alpha I_{in}\right)\left[\frac{3}{2}\left(16+\pi^2\right)\beta\sin\beta\right. \\
&\left.-4\pi^2\cos\beta - \frac{3}{2}\pi^2\frac{\epsilon_\perp}{\epsilon_a}\left(\beta\sin\beta + \frac{8}{\pi^2}\beta^2\cos\beta\right)\right] \\
&- B^2\left(\alpha I_{in}\right)^2\left[-2\pi^2\cos^2\beta + \frac{3}{4}\left(16+\pi^2\right)\beta\sin 2\beta\right. \\
&\left.+\frac{\epsilon_\perp}{\epsilon_a}\left(\frac{3}{4}\pi^2\beta\sin 2\beta + 12\cos 2\beta\right)\right]
\end{aligned}$$

$$\begin{aligned}
\frac{\gamma}{\epsilon_a}c_5 = &\frac{2}{15}\frac{\pi^2}{d^2}\frac{K}{\epsilon_a} \\
&- B\alpha I_{in}(\tilde{E}_0 + A\alpha I_{in})\left[(16+2\pi^2)\beta^2\cos\beta\right. \\
&+\left(\frac{1}{3}\left(16+\frac{3}{8}\pi^2\right)\beta\sin\beta\right. \\
&\left.\left.+\frac{\epsilon_\perp}{\epsilon_a}(32\beta^2\sin\beta - \pi^2\cos\beta)\right]\right. \\
&- B^2(\alpha I_{in})^2\left[16+2\pi^2\right)\beta^2\cos 2\beta \\
&+\frac{1}{6}\left(16+\frac{3}{8}\pi^2\right)\beta\sin 2\beta \\
&\left.+\frac{\epsilon_\perp}{\epsilon_a}\left(16\beta^2\sin 2\beta - 2\pi^2\beta^2\cos 2\beta\right)\right]. \qquad \text{(A.1)}
\end{aligned}$$

The first terms (first lines, r.h.s.) are the usual expressions, when there is no feedback correction. In particular, by setting $c_1 = 0$ we recover the threshold for the Fréedericksz transition:

$$\tilde{E}_{0F} = \frac{\pi}{d}\sqrt{\frac{K}{\epsilon_a}}.$$

When the feedback is added, there are extra terms proportional to the input light intensity I_{in}. More precisely, αI_{in} is the additional electric field applied to liquid crystal film in the presence of light on the photoconductor. The geometric factors, due to the specific choice of the polarization angles, are included in the A and B coefficients whereas the terms in β describe the phase shift experienced by the light which has passed through the liquid crystal film.

In the presence of the light feedback, and depending on the specific values of A and B (i.e. on the choice of the polarization angles ψ_1 and ψ_2), c_3 can change sign at the bifurcation point, thus leading to a subcritical Fréedericksz transition. However, when c_3 becomes positive c_5 remains negative, so that the saturation of the amplitude is assured.

References

1. See e.g. L. Kramer, W. Pesch, in *Pattern Formation in Liquid Crystals*, edited by A. Buka, L. Kramer (Springer-Verlag, New York, 1996)
2. N.V. Tabiryan, A.V. Sukhov, B.Ya. Zel'dovich, Mol. Cryst. Liq. Cryst. **136**, 1 (1986)
3. Special issue *Pattern Formation in Nonlinear Optical Systems*, edited by R. Neubecker, T. Tschudi, Chaos, Solitons & Fractals **10** (4-5) (1999); F.T. Arecchi, S. Boccaletti, P.L. Ramazza, Phys. Rep. **318**, 1 (1999)
4. F.T. Arecchi, S. Boccaletti, S. Ducci, E. Pampaloni, P.L. Ramazza, S. Residori, J. Nonlin. Opt. Phys. Mat. **9**, 183 (2000)
5. R. MacDonald, H.J. Eichler, Opt. Commun. **89**, 289 (1992)
6. E. Santamato, E. Ciaramella, M. Tamburrini, Mol. Cryst. Liq. Cryst. **251**, 127 (1994)
7. E. Louvergneaux, Phys. Rev. Lett. **87**, 244501 (2001)
8. V. Fréedericksz, V. Zolina, Trans. Faraday Soc. **29**, 919 (1933)
9. P.G. de Gennes, J. Prost, *The Physics of Liquid Crystals*, 2nd edn. (Oxford Science Publications, Clarendon Press, 1993)
10. S. Chandrasekhar, *Liquid Crystal* (Cambridge, New York, 1992)
11. M.O. Cáceres, F. Sagués, M. San Miguel, Phys. Rev. A **41**, 6852 (1990)
12. B.J. Frisken, P. Palffy-Muhoray, Phys. Rev. A **39**, 1513 (1989); Phys. Rev. A **40**, 6099 (1989)
13. S. Garg, S. Saeed, U.D. Kini, Phys. Rev. E **51**, 5846 (1995)
14. S.D. Durbin, S.M. Arakelian, Y.R. Shen, Phys. Rev. Lett. **47**, 1411 (1981); S.R. Nersisyan, N.V. Tabiryan, Mol. Cryst. Liq. Cryst. **116**, 111 (1984); A.J. Karn, S.M. Arakelian, Y.R. Shen, H.L. Ong, Phys. Rev. Lett. **57**, 448 (1986); E. Santamato, G. Abbate, R. Casaselice, P. Maddalena, A. Sasso, Phys. Rev. A **37**, 1375 (1988)
15. P.Y. Wang, H.J. Zhang, J.H. Dai, Opt. Lett. **12**, 654 (1987)

16. M.G. Clerc, S. Residori, C.S. Riera, Phys. Rev. E **63**, 060701 (2001)
17. R.A. Fisher, Ann. Eugenics **7**, 335 (1937)
18. A.N. Kolmogorov, J. Petrovsky, N. Piskunov, Bull. Univ. Moskou Ser. Int. Se. **7**(6), 1 (1937)
19. J.D. Murray, *Mathematical Biology* (Springer-Verlag, Berlin, 1993)
20. P. Kife, *Mathematical Aspects of Reacting and Diffusing System*, edited by S. Levin, Lecture Notes in Biomathematics (Springer-Verlag, New-York, 1979), Vol. 28
21. D. Walgraef, *Spatio-temporal pattern formation* (Springer-Verlag, New York, 1997)
22. G. Dee, J.S. Langer, Phys. Rev. Lett. **50**, 383 (1983)
23. P. Manneville, *Dissipative structures and weak turbulence* (Academic Press, San Diego, 1990)
24. M. Cross, P. Hohenberg, Rev. Mod. Phys. **65**, 581 (1993)
25. D.G. Aronson, H.F. Weinberger, Adv. Math. **30**, 33 (1978)
26. P. Collet, J.P. Eckmann, *Instabilities and fronts in extended system* (Princeton University Press, New Jersey, 1990)
27. P.L. Ramazza, S. Ducci, F.T. Arecchi, Phys. Rev. Lett. **81**, 4128 (1998); J. Bragard, P.L. Ramazza, F.T. Arecchi, S. Boccaletti, L. Kramer, Phys. Rev. E **61**, R6045 (2000)
28. E. Yao, F. Papoff, G.L. Oppo, Phys. Rev. E **59**, 2918 (1999)
29. L.D. Landau, E.M. Lifshitz, *Statistical physics* (Pergamon Press, New York, 1969)
30. W.K. Burton, N. Cabrera, F.C. Frank, Phil. Trans. Roy. Soc. Lond. A **243**, 299 (1951)
31. Y. Pomeau, Physica D **23**, 3 (1986)
32. S.A. Akhmanov, M.A. Vorontsov, V.Yu. Ivanov, JETP Lett. **47**, 707 (1988)
33. S. Residori, A. Petrossian, L. Gil, Phys. Rev. Lett. **88**, 233901-1 (2002)